Fluid Phase Equilibria 429 (2016) 242–253

Contents lists available at ScienceDirect

Fluid Phase Equilibria

journal homepage: www.elsevier.com/locate/fluid

Binary Lennard-Jones mixtures with highly asymmetric interactions of the components. 1. Effect of the energy parameters on phase equilibria and properties of liquid-gas interfaces

Sergey P. Protsenko*, Vladimir G. Baidakov

Institute of Thermophysics, Ural Branch of the Russian Academy of Sciences, Amundsen street 107a, 620016, Ekaterinburg, Russia

ARTICLE INFO

Article history:
Received 29 June 2016
Received in revised form
30 August 2016
Accepted 5 September 2016
Available online 7 September 2016

Keywords:
Molecular dynamics simulation
Lennard-Jones mixture
Phase equilibria liquid-gas
Orthobaric densities
Surface tension
Saturation pressure
Relative absorption

ABSTRACT

The molecular dynamics method has been used to investigate liquid-gas phase equilibria in two-component systems containing up to 117000 Lennard-Jones particles. The parameters of the interaction potentials of the mixture components differed only in the ratio of the interaction energies $\varepsilon_{22}/\varepsilon_{11}$, which varied from 0.1 to 0.2. Systems with such interaction parameters simulate solutions with limited solubility, in which the second component plays the role of a volatile impurity. The orthobaric densities, saturation pressure, surface tension γ, relative adsorption $\Gamma_{2(1)}$, and the effective interface thickness have been calculated as functions of the concentration of volatile component in the liquid phase c_l in the range of reduced temperatures from $T^* = k_BT/\varepsilon_{11} = 0.6$ to 1.0. An increase in the adsorption of the volatile component with increasing ratio $\varepsilon_{22}/\varepsilon_{11}$ has been established. The isotherms $\Gamma_{2(1)}(c_l)$ and $\gamma(c_l)$ have the following extreme points: maximum $\Gamma_{2(1)}(c_l)$ and minimum $\gamma(c_l)$, whose positions do not coincide.

1. Introduction

The interaction of nonpolar molecules is satisfactorily described by the Lennard-Jones (LJ) pair potential. The potential parameters are the minimum energy of interaction of two particles ε and the effective particle diameter σ. The LJ potential is used in the studies of both one-component and multicomponent systems in one- and two-phase states. In a binary system, besides the parameters of individual components $\varepsilon_{\alpha\alpha}$ and $\sigma_{\alpha\alpha}$, where $\alpha = 1$ or 2, it is necessary to know the parameters of the interaction of particles of different species: $\varepsilon_{\alpha\beta}$, $\sigma_{\alpha\beta}$. By varying the ratios between sizes, energy parameters and particle masses m_α, it is possible to design solutions with different physicochemical properties. To investigate the phase behavior and the properties of the interface of binary mixtures, use was made of the Monte Carlo (MC) and molecular dynamics (MD) methods [1–4], and molecular-statistical theories [5–10]. Along with methods of molecular simulation, powerful tools for the study of interfacial properties are the density gradient theory (DGT) [11–14] and the density functional theory (DFT) [15–19].

Both MD and MC simulations, and also DGT and DFT methods in investigations of two-phase systems allow determining saturation pressure, orthobaric densities, phase composition, and also partial density profiles, the thickness of an interfacial layer, the positions of interfaces, profiles of components of pressure tensor, relative adsorption, and surface tension.

The DGT is the development of the theory of inhomogeneous fluids by van der Waals [11]. The free energy density is written as a Taylor series limited by two terms. The first term is calculated at every value of the local density. The equation of state of a bulk fluid is used for this purpose. The density profile is taken into account to the second square-gradient term. A limitation of the DGT method is the use of the influence parameters, i.e. coefficients of square-gradient expansion terms. The influence parameters are determined on the basis of experimental data on the surface tension of pure fluids, and then are applied to mixtures.

The idea of the DFT method consists in calculation of the free energy functional for an inhomogeneous system with a subsequent calculation of surface tension. The functional consists of two parts: the reference term includes ideal and short-range interactions, and the term that describes perturbations includes long-range interactions. The reference term can be based on different approximations.

* Corresponding author.
E-mail address: sp@itp.uran.ru (S.P. Protsenko).

http://dx.doi.org/10.1016/j.fluid.2016.09.009
0378-3812/

In both approaches the evaluation of the bulk properties of phases requires an equation of state. The free energy in the DGT depends on the equation of state used and the influence parameters. In the DFT approximation the functional depends on the free energy approximation used.

MD and MC models are determined only by the interaction potentials of the mixture particles. In the case of Lennard-Jones interactions the model parameters are only particle masses, values of the minimums of potential wells, and effective sizes of the particles of components. Then the properties of inhomogeneous systems being simulated are determined by the inherent dynamics of particles (MD method), and the selection of states corresponding to a minimum of the thermodynamic potential in a given statistical ensemble (MC method). The results of simulation by both methods are, as a rule, closely analogous. Thus, at a given interaction potential the results of the MD and MC simulations are rigorous and may be used for testing molecular-statistical theories of solutions.

The effect of the ratio of energy parameters of interaction $\varepsilon_{22}/\varepsilon_{11}$ of the components of a binary LJ mixture on phase equilibria and properties of a liquid-gas interface was investigated in Refs. [5–7,19]. The density functional mean-field approximation (DFT-MFT) was used in Ref. [19]. The results of analytical calculations have been compared with data from MD simulations. It has been found in Ref. 19 that the DFT-MFT underestimates the values of bulk liquid density ρ_l (by 10%) and the surface tension γ (by 15%), but describes with a sufficient precision the shape of the density profile at the interface: both the width of an interfacial layer and the value of adsorption are in a good agreement with the results of MD simulations. Parameters of phase equilibrium in binary LJ mixtures have been calculated in the framework of van der Waals l-fluid theory of solutions in Refs. [5–7]. The results of calculations are in satisfactory agreement with data of simulations by MC method [20–22]. With increasing differences in the values of interaction parameters the agreement deteriorates.

In real solutions, the value of the ratio of energy parameters may vary over a wide range. Thus, in the CH_4–H_2 solution, the ratio $\varepsilon_{22}/\varepsilon_{11} \approx 0.2$, C_2H_6–H_2: $\varepsilon_{22}/\varepsilon_{11} \approx 0.12$, CH_4–He: $\varepsilon_{22}/\varepsilon_{11} \approx 0.04$, and C_2H_6–He: $\varepsilon_{22}/\varepsilon_{11} \approx 0.024$ [23].

In the present paper, the MD method is used to investigate two-component two-phase LJ mixtures with ratios of energy parameters of interaction $\varepsilon_{22}/\varepsilon_{11}$ from 0.1 to 0.2, i.e. with a degree of the asymmetry of interactions exceeding that in Refs. [5–7,19], where the ratio $\varepsilon_{22}/\varepsilon_{11}$ was 0.25–0.7. Calculations were done in the temperature range from $k_BT/\varepsilon_{11} = 0.6$ to 1.0. The particles were of the same size and mass. The cutoff radius of the potential was taken equal to $r_c^* = r/\sigma_{11} = 6.78$. As shown in Ref. [24], the choice of $r_c^* > 6$ ensures an adequate, cutoff-radius-independent reproduction of both the properties of bulk phases and those of the interface. The value of $r_c^* \leq 2.5$ used in Refs. [2,4–10,18,19] leads to an underestimation of orthobaric densities of 10–20%, and that of surface tension of 40–60% as compared with the full potential. To allow for the wide spectrum of capillary waves at a plane interface, its area in the present paper exceeds that in Refs. [1–4,18,19] approximately 10 times.

The paper is organized as follows. The second section describes the MD model. The third presents the results of simulation of two-phase systems with ratios of interaction parameters $\varepsilon_{22}/\varepsilon_{11} = 1/10$, 1/7 and 1/5. The results of the investigation conducted are discussed in the fourth section. The fifth, presents brief conclusion.

2. Molecular dynamics model

The interactions between particles in two-component systems were described by the LJ potential

$$\phi_{\alpha\beta}(r) = \begin{cases} 4\varepsilon_{\alpha\beta}\left[\left(\frac{\sigma_{\alpha\beta}}{r}\right)^{12} - \left(\frac{\sigma_{\alpha\beta}}{r}\right)^{6}\right], & r < r_c \\ 0, & r \geq r_c \end{cases}. \quad (1)$$

At $r_c = 6.78\sigma_{11}$ the value of $\phi_{11}/\varepsilon_{11} \approx 4.1 \cdot 10^{-5}$, therefore corrections for interactions at $r > r_c$ were not introduced.

The results of calculations are presented in a dimensionless form. For units of energy, length, and mass use was made of the parameters of the first component of the mixture ε_{11}, σ_{11}, m_1. The reduced temperature was determined as $T^* = k_BT/\varepsilon_{11}$, pressure as $p^* = p\sigma_{11}^3/\varepsilon_{11}$, density as $\rho^* = \rho\sigma_{11}^3$, surface tension as $\gamma^* = \gamma\sigma_{11}^2/\varepsilon_{11}$, and adsorption as $\Gamma^* = \Gamma\sigma_{11}^2$. The unit of time was $\sigma_{11}(m_1/\varepsilon_{11})^{1/2}$. The cross interactions between unlike species were calculated by the mixing rules of Berthelot $\varepsilon_{12} = (\varepsilon_{11}\varepsilon_{22})^{1/2}$ and Lorentz $\sigma_{12} = (\sigma_{11} + \sigma_{22})/2$.

The particles of the mixture were placed in a cell which had the form of a rectangular parallelepiped. The cell volume was $V = L_x \times L_y \times L_z$, where $L_x = L_y = 40\sigma_{11}$, and the value of L_z varied from $75\sigma_{11}$ to $100\sigma_{11}$. Periodic boundary conditions acted in the directions of the axes of the Cartesian coordinate system x, y, and z. At the center of the cell formed a liquid layer with a thickness $L_z/2$ surrounded on two sides by vapor-phase layers with a thickness $L_z/4$. The number of particles in the cell N varied from 56000 to 117000. Calculations were made in the NVT ensemble with an integration step of the equations of motion $\Delta t^* = 0.002318$. The temperature constancy was ensured by the Nose-Hoover thermostat [25–27]. An equilibrium composition in the bulk phases and the transition layer was formed in the process of equilibration of the initial state ($T = \text{const}$). The time of equilibration ranged from a few hundreds to several millions of time steps.

After the establishment of the equilibrium state the profiles of local number density $\rho(z)$, energy density $u(z)$, temperature $T(z)$, the normal $P_N(z)$ and tangential $P_T(z)$ components of pressure tensor [28] were calculated. For calculating the profiles of the quantities mentioned the cell was divided into layers of thickness $\Delta z^* = \Delta z/\sigma_{11} = 0.05$.

The number density in the layer with number n will look like

$$\rho(z_n) = N(z_n)/\Delta V, \quad (2)$$

where $N(z_n)$ is the number of particles in the layer $(z_n - \Delta z/2, z_n + \Delta z/2)$ and $\Delta V = L_xL_y\Delta z$ is the layer volume.

For the density of potential energy we have

$$u(z_n) = \sum_i \sum_j \phi_{\alpha\beta}(r_{ij})/\Delta V, \quad (3)$$

where r_{ij} is the distance between particles i and j, summation with respect to i is carried out over all the particles in the layer with number n. The energy of every particle in the layer was determined by its interaction with all the particles of the system, and not just the layer particles.

The temperature profile was calculated as

$$T(z_n) = \sum_i m\upsilon_i^2 \Big/ (3k_BN(z_n)). \quad (4)$$

Here υ_i is the velocity of the i-th particle in the n-th layer.

The normal and tangential components of the pressure tensor will look like

$$P_N(z_n) = \langle \rho(z_n) \rangle k_B T - \frac{1}{A} \left\langle \times \sum_{ij} \frac{z_{ij}^2}{r_{ij}} \frac{d\phi(r_{ij})}{dr_{ij}} \frac{1}{|z_{ij}|} \theta\left(\frac{z_n - z_i}{z_{ij}}\right) \theta\left(\frac{z_j - z_n}{z_{ij}}\right) \right\rangle, \quad (5)$$

$$P_T(z_n) = \langle \rho(z_n) \rangle k_B T - \frac{1}{A} \left\langle \times \sum_{ij} \frac{x_{ij}^2 + y_{ij}^2}{2r_{ij}} \frac{d\phi(r_{ij})}{dr_{ij}} \frac{1}{|z_{ij}|} \theta\left(\frac{z_n - z_i}{z_{ij}}\right) \theta\left(\frac{z_j - z_n}{z_{ij}}\right) \right\rangle, \quad (6)$$

where A is the surface area of one interface, x_{ij}, y_{ij}, and z_{ij} are the separations of particles i and j, and $< \ldots >$ denotes NVT ensemble average, $\theta(x)$ is the unit step-function.

Owing to the nonuniformity of the evaporation of particles from interfaces, a liquid film in the process of evolution of the system might shift along the z-axis. In the course of the MD simulation its position was corrected. The origin of reading of the profiles of $\rho(z)$, $u(z)$, $T(z)$, $P_N(z)$ and $P_T(z)$ was related to the axis of symmetry of the liquid phase.

The functions $\rho(z)$, $u(z)$, $T(z)$, $P_N(z)$, and $P_T(z)$ were obtained by averaging over $1 \cdot 10^6$ steps. The orthobaric densities of liquid ρ_l, gas ρ_g, and the saturation pressure p_s were determined from distributions of $\rho(z)$ and $P_N(z)$. The surface tension was calculated in accordance with its mechanical definition

$$\gamma = \frac{1}{2} \int_{-\infty}^{+\infty} [P_N(z) - P_T(z)] dz. \quad (7)$$

The factor 1/2 appears due to the presence of two interfaces in the system.

The relative adsorption of the second component at the equimolecular dividing surface of the first component $z_{1,e}$ is [19].

$$\Gamma_{2(1)} = \int_0^{z_{1,e}} \left(\rho_2(z) - \rho_{2,l}\right) dz + \int_{z_{1,e}}^{L_z/2} \left(\rho_2(z) - \rho_{2,g}\right) dz. \quad (8)$$

Here $\rho_2(z)$ is the partial density profile of the second component, and $\rho_{2,l}$, $\rho_{2,g}$ is the partial density of the second component in the bulk liquid l and gas g phases.

The effective thickness of the interface L_{10}^{90} was determined according to [29], as the distance at which the density varied from $\rho_{10} = \rho_g + 0.1\Delta\rho$ to $\rho_{90} = \rho_g + 0.9\Delta\rho$, where $\Delta\rho = \rho_l$ - ρ_g.

The average concentration of the second component in the mixture is

$$<c> = N_2/N, \quad (9)$$

where N_2 is the number of particles of the second component in the system.

The concentration (molar fraction) of the second component in the bulk liquid and gas will look like

$$c_l = \rho_{2,l}/\rho_l \text{ and } c_g = \rho_{2,g}/\rho_g. \quad (10)$$

3. Simulation results

3.1. Structure of two-phase systems

Solutions in which the ratios of the energy parameters of the LJ potential were $\varepsilon_{22}/\varepsilon_{11} = 1/10$, 1/7, and 1/5 and a one-component system with $\varepsilon_{22}/\varepsilon_{11} = 1$ have been investigated. The particle sizes of the first and the second component, and also their masses had the same values. The potentials of interparticle interaction of the solution components are presented in Fig. 1.

Calculations were carried out at temperatures $T^* = 0.6$, 0.7, 0.8, 0.9, 1.0 and several values of the mixture compositions. The critical temperature of the first component was $T_{1,c}^* = 1.331$ [24]. The critical temperature of the second component is determined as $T_{1,c}^* \varepsilon_{22}/\varepsilon_{11}$. An addition of a volatile impurity into a two-phase system leads to an increase in its concentration in the gas phase and increase of the saturation pressure. The particles with a strong interaction energy are mainly localized in the liquid phase. At such a redistribution of particles of different kinds one more possibility of reducing the energy of two-phase system is connected with the adsorption of the volatile component in the surface layer and the decrease of the surface tension.

Fig. 2 shows a projection of particles in the cell on the plane yz for a two-phase system with $\varepsilon_{22}/\varepsilon_{11} = 0.2$, an average concentration of the second component $<c> = 0.39$ and $T^* = 0.9$. The particles of the first component are mainly located in the central part of the cell (Fig. 2b), where the mixture density is higher (Fig. 2a). For the most part, a gas phase consists of particles of the second component with weaker interparticle interactions (Fig. 2c). Cross interactions with $\varepsilon_{12} \approx 0.447\varepsilon_{11}$ ensure a sufficiently high content of particles of species 2 in a liquid phase ($c_l = 0.109$), and those of species 1 in a gas phase ($(1 - c_g) = 0.186$). The profiles of the number density and the density of the potential energy in this state are presented in Fig. 3.

Fig. 4 illustrates the evolution of a total $\rho^*(z^*)$ and a partial $\rho_2^*(z^*)$ density profiles for a mixture with $\varepsilon_{22}/\varepsilon_{11} = 0.2$ at $T^* = 0.9$ with increasing concentration of the second component in the liquid. The horizontal sections of the profiles $\rho^*(z^*)$ determine the values

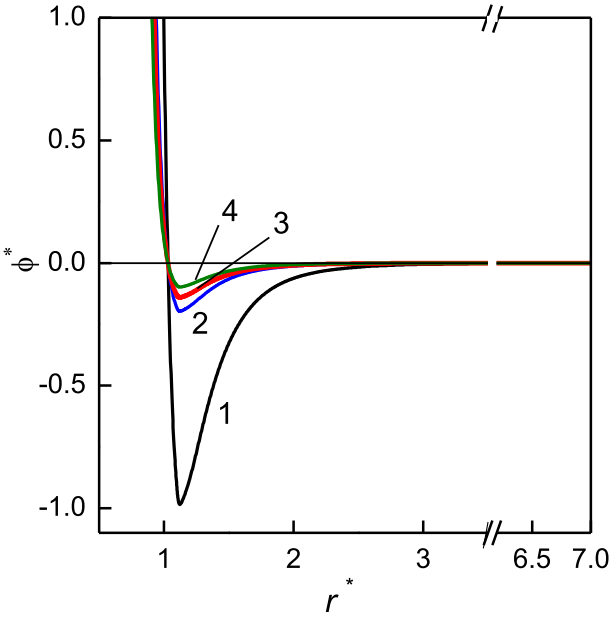

Fig. 1. Interaction energy of components with a different depth of the potential well: (1) $\varepsilon_{22}/\varepsilon_{11} = 1$; (2) 1/5; (3) 1/7; (4) 1/10.

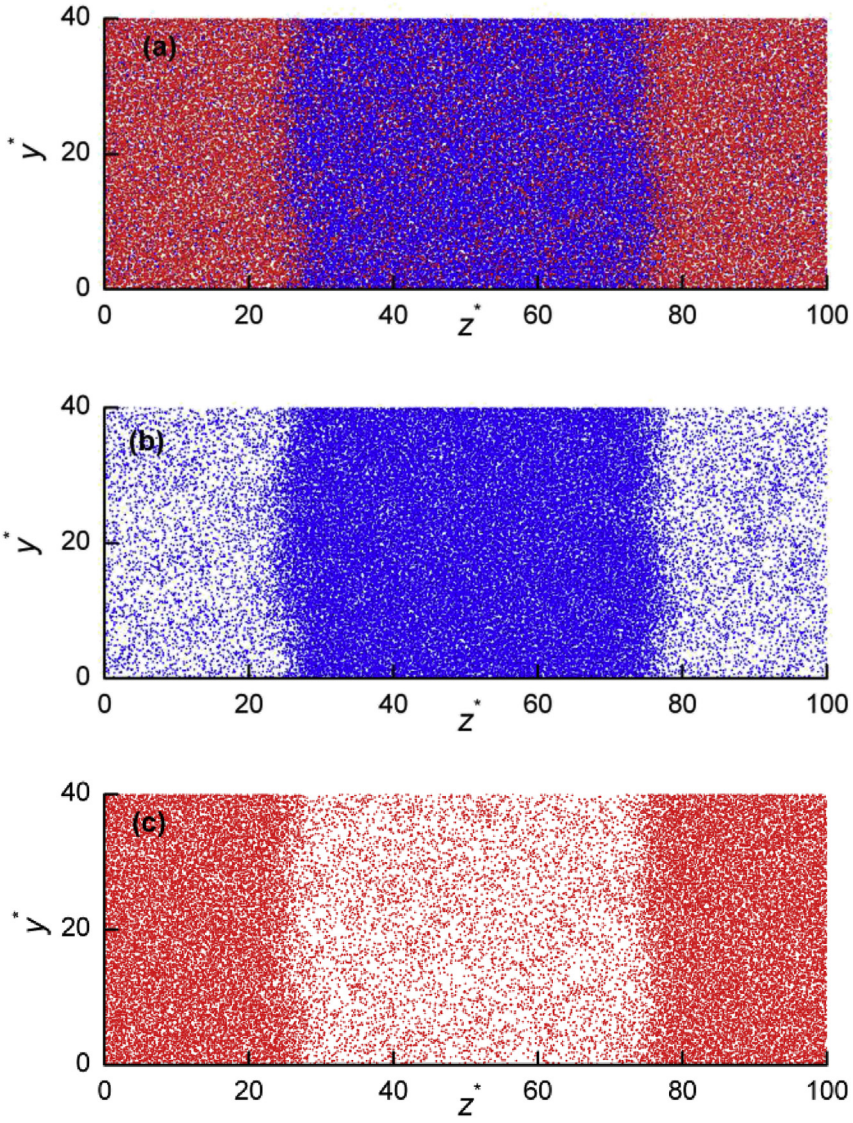

Fig. 2. Projection of the position of particles in a cell in a mixture with $\varepsilon_{22}/\varepsilon_{11} = 1/5$ in a state of two-phase equilibrium at $T^* = 0.9$ and $c_l = 0.109$: (a) particles of the first (blue dots) and second (red dots) components, $N = 104400$; (b) the first component, $N_1 = 64000$; (c) the second component, $N_2 = 40400$. (For interpretation of the references to colour in this figure legend, the reader is referred to the web version of this article.)

of orthobaric densities of the liquid ρ_l^* and the gas ρ_g^* phases. The increase of ρ_l^* is caused by the increase in the partial density of the second component $\rho_{2,l}^*$ (see the inset in Fig. 4). In this case the concentration of the first component in the bulk liquid and the partial density $\rho_{1,l}^*$ decrease. A further increase in the content of the second component in the system leads to the convergence of the densities of the liquid and gas phases as the rate of growth of ρ_g^* is ahead of the rate of growth of ρ_l^*. In range of c_l from 0.0083 to 0.0667 the profiles of $\rho_2^*(z^*)$ have maximums which point to the enrichment of the interfacial layer with the second component.

The maximums on the partial profiles of a volatile component have been obtained by both MD simulation and investigation by the DFT method of LJ mixtures with variable interaction parameters [19], in the MD model of Ar-Ne [3], and also in calculating interfacial properties by the DGT technique in H_2O–CO_2 [30–35], H_2O–H_2S [34], H_2O–CH_4 [32,33] mixtures. Moreover, the decay and disappearance of the peak on the density profile of the component with relatively weaker interparticle interactions have been revealed at high values of the equilibrium pressure (volatile component concentration) [14,32] as well as in our systems.

The effect of the value of $\varepsilon_{22}/\varepsilon_{11}$ on the distribution of components in bulk phases and the interfacial layer is shown in Fig. 5, where the profiles of densities are presented for three values of $\varepsilon_{22}/\varepsilon_{11}$ at $T^* = 0.7$. In systems of the one average composition $<c> = 0.377$ the partial densities of the components in bulk phases do not differ by more than 3% (Fig. 5a). At a fixed composition of the liquid phase ($c_l \approx 0.0085$) the partial density of the first component in the liquid and the second in the gas are higher when $\varepsilon_{22}/\varepsilon_{11}$ is lower (Fig. 5b). The enrichment of the transition layer with the second component decreases as the ratio $\varepsilon_{22}/\varepsilon_{11}$ is decreased.

3.2. Phase equilibrium parameters

The concentration dependences of orthobaric densities and saturation pressure at $T = \text{const}$ are presented in Figs. 6 and 7. The variation of the ratio of energy parameters of interaction leads to qualitative changes in phase diagrams (see Fig. 6). At all temperatures in a solution with $\varepsilon_{22}/\varepsilon_{11} = 0.1$ the equilibrium density of the

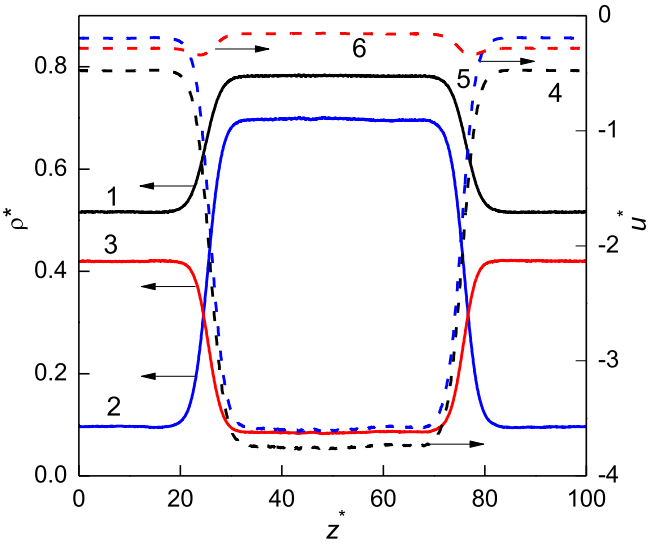

Fig. 3. Profiles of number density $\rho^*(z^*)$ (solid lines) and density of potential energy $u^*(z^*)$ (dashed lines) in a state of two-phase equilibrium in a mixture with $\varepsilon_{22}/\varepsilon_{11} = 0.2$ at $T^* = 0.9$ and $c_l = 0.109$: (1, 4) total number density and potential energy density (black lines); (2, 5) the first component (blue lines); (3, 6) the second component (red lines). (For interpretation of the references to colour in this figure legend, the reader is referred to the web version of this article.)

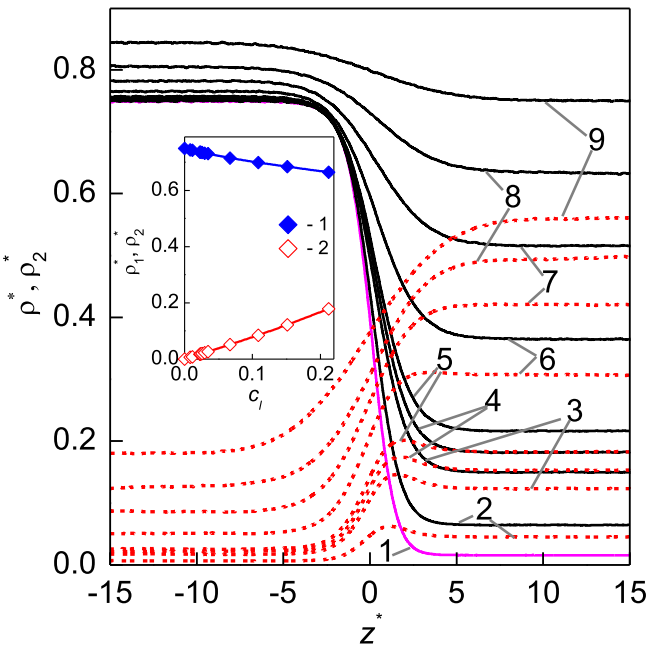

Fig. 4. Evolution of density profiles in a mixture with $\varepsilon_{22}/\varepsilon_{11} = 0.2$ at $T^* = 0.9$ with an increase of the concentration of the second component in the liquid phase: (1) $c_l = 0$; (2) 0.0083; (3) 0.0235; (4) 0.0295; (5) 0.0345; (6) 0.0667; (7) 0.1088; (8) 0.1512; (9) 0.2121. Solid lines show total density profiles of a one-component ($c_l = 0$) and a two-component systems, dashed lines those of the second component. The position of the equimolecular dividing surface of a one- and the two-component systems has been chosen as a reference point on the z-axis. The inset shows concentration dependences of the partial densities of the first (1) and the second (2) component in the liquid phase.

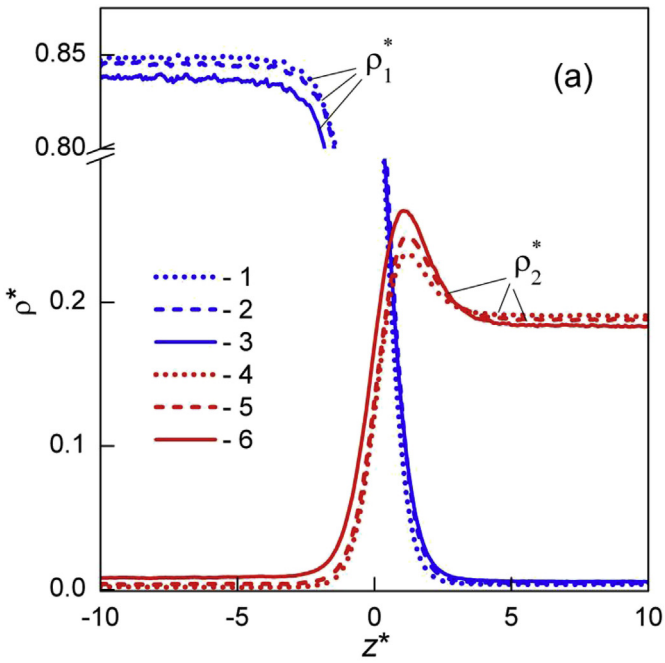

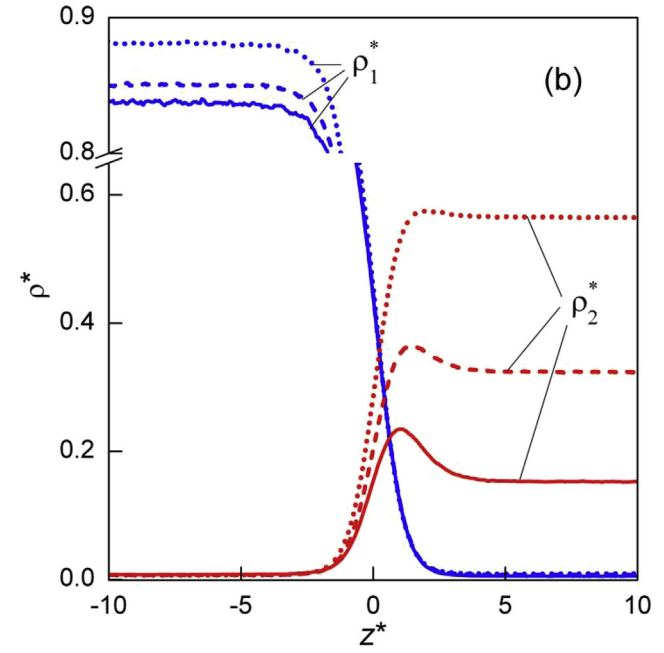

Fig. 5. Partial density profiles of the first $\rho_1^*(z^*)$ (blue lines) and second $\rho_2^*(z^*)$ (red lines) components in solutions with the following ratios of energy parameters: (1, 4) $\varepsilon_{22}/\varepsilon_{11} = 1/10$; (2, 5) 1/7; (3, 6) 1/5 at temperature of $T^* = 0.7$, when the average concentration of the second component in the system <c> = 0.377 (a) and the concentration of the second component in the bulk liquid $c_l \approx 0.0085$ (b). (For interpretation of the references to colour in this figure legend, the reader is referred to the web version of this article.)

liquid increases abruptly with a growth in the concentration of the second component. An increase in the ratio $\varepsilon_{22}/\varepsilon_{11}$ leads to deceleration of the dependences $\rho_l^*(c_l)$. At a fixed value of $\varepsilon_{22}/\varepsilon_{11}$ the higher the temperature, the smaller the slope of the dependences $\rho_l^*(c_l)$. Thus, in a mixture with $\varepsilon_{22}/\varepsilon_{11} = 0.2$ at $T^* = 1$ the liquid density is practically independent of c_l, i.e. it is permissible to considerably increase the content of the second component in the liquid, which is accompanied by displacement of particles of the first component into the gas phase. In this case the growth of the orthobaric density of the gas also takes place at the expense of the increase in it of number of particles of the first component with a simultaneous reduction in the concentration of the second component. The derivative of $\rho_g^*(c_g)$ with respect to c_g changes the

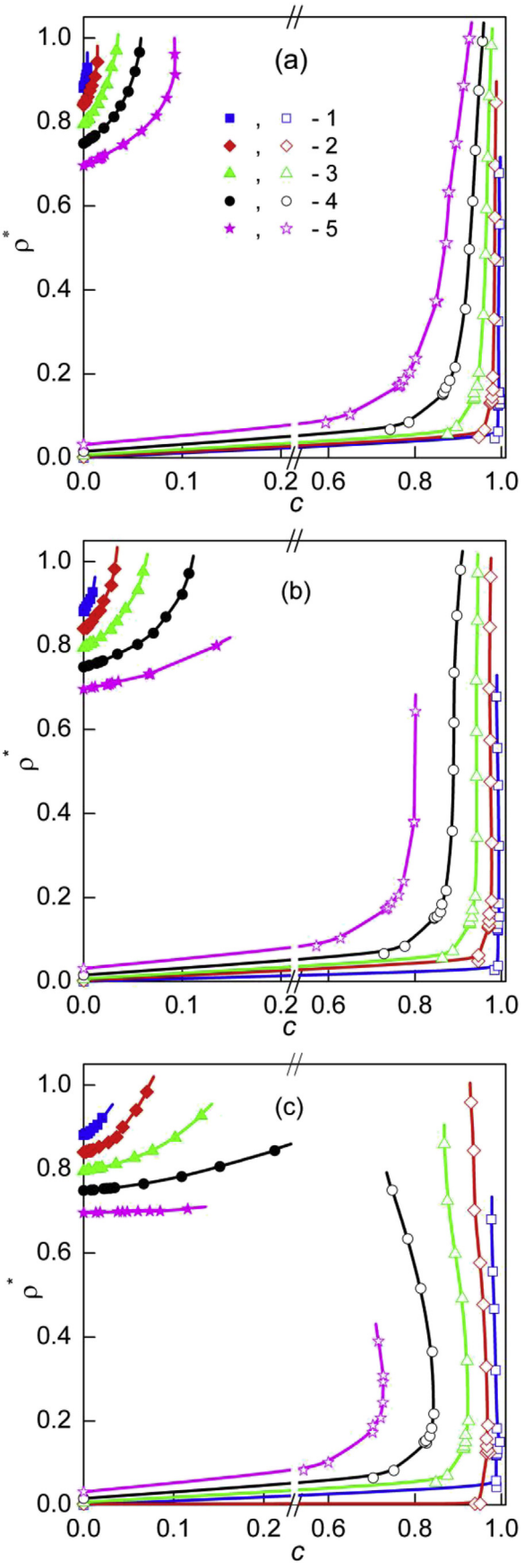

sign from positive to negative. A situation arises in which at one value of the temperature in equilibrium with the liquid phase there may be a fluid at two values of the density, but at one concentration of the second component c_g.

From Fig. 7 it follows that an increase in the content of the volatile component in the liquid results in a considerable increase of the saturation pressure p_s^*. The value of p_s^* in a solution may be two or three orders higher than in one-component system at the same temperature. Thus, at $T^* = 1$ in a mixture with $\varepsilon_{22}/\varepsilon_{11} = 0.1$ the largest value of the saturation pressure is $p_s^*(c_l = 0.0924) = 5.533$, whereas in a one -component system $p_s^*(c_l = 0) = 0.0264$. At a temperature $T^* = 0.7$ in a mixture with $\varepsilon_{22}/\varepsilon_{11} = 0.2$ the highest pressure of phase equilibrium is $p_s^*(c_l = 0.07) = 4.098$, and at $\varepsilon_{22}/\varepsilon_{11} = 1$ $p_s^*(c_l = 0) = 0.0015$. At $\varepsilon_{22}/\varepsilon_{11} = 0.2$ the isotherms $p_s^*(c)$ of the gas phase admit the possibility of liquid-gas equilibrium at one value of c_g and two values of pressure.

The content of the volatile component in the liquid phase increases with the growth of $\varepsilon_{22}/\varepsilon_{11}$. The effect the ratio $\varepsilon_{22}/\varepsilon_{11}$ on the concentration dependence of orthobaric densities and the saturation pressure at temperatures $T^* = 0.7$ and 0.9 is shown in Fig. 8. Thus at a temperature $T^* = 0.9$ limiting attainable concentrations of the volatile component in the liquid c_l change from 0.057 to 0.212 as $\varepsilon_{22}/\varepsilon_{11}$ varies from 0.1 to 0.2. The larger $\varepsilon_{22}/\varepsilon_{11}$, the lower is the orthobaric density of the liquid and the saturation pressure. With a large amount of the volatile component in the system the densities of coexistent liquid and gas phases become comparable. These phases differ in composition rather than in density. The liquid phase contains 80–95% of the first component, and in the gas phase values close to this are achieved for the concentration of the second component. Such a distribution of particles ensures an energy density of the liquid phase that is almost an order of lower as compared with the gas phase (Fig. 3).

The critical temperature of the second component in the investigated mixtures at the same masses and particle sizes may be evaluated as $T_{2,c}^* = T_{1,c}^* \varepsilon_{22}/\varepsilon_{11}$. If $T_{1,c}^* = 1.331$ [24], then at $0.1 \le \varepsilon_{22}/\varepsilon_{11} \le 0.2$ $0.133 \le T_{2,c}^* \le 0.266$. Thus, in the temperature range $0.6 \le T^* \le 1.0$ the second component is in a supercritical state and cannot undergo a phase transition. At the high pressures achieved in the investigated mixtures and the prescribed temperature range a gas-liquid phase transition leading to liquid-liquid equilibrium might take place at $\varepsilon_{22}/\varepsilon_{11}$ of no less than 0.5. More likely we might speak about the transition of the solution into the liquid state. However, at the concentration of the volatile component in the external ("gas") phase of 0.6 or over the solution is also in a supercritical state. Thus, in all the investigated states of two-phase equilibrium we had the equilibrium of a liquid phase rich in the first component and a phase rich in the volatile component, which was in a state of supercritical fluid.

3.3. Interface properties

Fig. 9 presents the isotherms of the concentration dependences of the surface tension calculated according to Eq. (7). In a mixture with $\varepsilon_{22}/\varepsilon_{11} = 1/5$ (Fig. 9c) at all temperatures $\gamma^*(c_l)$ is a monotonically decreasing function of concentration. With decreasing ratio $\varepsilon_{22}/\varepsilon_{11}$ the behavior of functions $\gamma^*(c_l)$ changes qualitatively. When $\varepsilon_{22}/\varepsilon_{11} = 1/7$ on the $\gamma^*(c_l)$ isotherms appear sections with a slope close to zero, and when $\varepsilon_{22}/\varepsilon_{11} = 1/10$ at $T^* > 0.6$ there is an increase in dependencies $\gamma^*(c_l)$ after passing of minimums (Fig. 9b,

Fig. 6. Dependences of orthobaric densities of a liquid (solid symbols) and a gas (open symbols) on the concentration of the second component for solutions with the following ratios $\varepsilon_{22}/\varepsilon_{11}$: (a) $\varepsilon_{22}/\varepsilon_{11} = 1/10$; (b) 1/7; (c) 1/5 at temperatures: (1) $T^* = 0.6$; (2) 0.7; (3) 0.8; (4) 0.9; (5) 1.0.

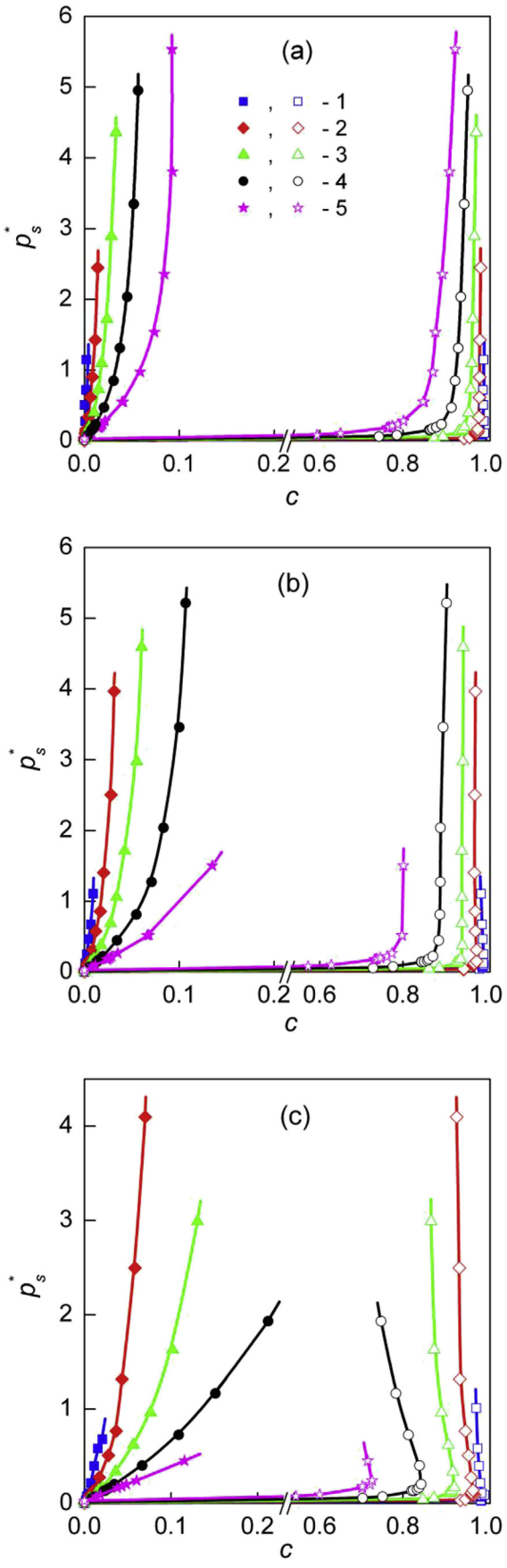

Fig. 7. Dependences of saturation pressure on the concentration of the second component in a liquid and a gas phase. For symbols see Fig. 6.

a).

The relative adsorption of the second component at temperatures $T^* = 0.7$ and 0.9 is presented in Fig. 10. The functions $\Gamma^*_{2(1)}(c_l)$ have the maximums at some c_l. When the content of the second component in the system grows further, the particles of the volatile component penetrate into the bulk liquid (Fig. 4) and the relative adsorption decreases. The value of maximum increases approximately two times with a change in the ratio $\varepsilon_{22}/\varepsilon_{11}$ from 0.1 to 0.2. In this case the maximums of $\Gamma^*_{2(1)}(c_l)$ shift towards higher concentrations. At fixed $\varepsilon_{22}/\varepsilon_{11}$ the maximum value of the relative adsorption decreases with the growth of the temperature.

Fig. 10 shows the behavior of the isotherms $\gamma^*(c_l)$ and $\Gamma^*_{2(1)}(c_l)$. At a temperature $T^* = 0.7$ (Fig. 10a) the surface tension decreases not only in the sections where $\Gamma^*_{2(1)}(c_l)$ increases, but also where it reduces after passing through the maximum. Here the derivative $(\partial\gamma/\partial c_l)_T$ is reduced to values close to zero. The function $\gamma^*(c_l)$ behaves similarly at a higher temperature $T^* = 0.9$, too, when $\varepsilon_{22}/\varepsilon_{11} = 0.2$ (Fig. 10b). In systems with $\varepsilon_{22}/\varepsilon_{11} = 1/7$ and 1/10 ($T^* = 0.9$) the dependences $\gamma^*(c_l)$ ($\gamma^*(p_s^*)$) become nonmonotonic: with increasing c_l (p_s^*) the surface tension passes through a minimum and increases further. The positions of maximums $\Gamma^*_{2(1)}(c_l)$ and minimums of $\gamma^*(c_l)$ do not coincide.

According to the mechanical definition of surface tension (Eq. (7)), the value of γ is influenced by the thickness of the interface and the value of deviation of the function $P_N^*(z^*)$-$P_T^*(z^*)$ from zero within the transition layer. At a temperature $T^* = 0.9$ the concentration dependence of the effective thickness of the interface L_{10}^{*90} is close to linear and does not practically depend on the ratio $\varepsilon_{22}/\varepsilon_{11}$ (Fig. 11). At $T^* = 0.9$ on the interval of concentrations c_l from 0 to 0.02 the values of $\gamma^*(c_l)$ are also independent of the ratio $\varepsilon_{22}/\varepsilon_{11}$ for the mixtures investigated (see Fig. 10b), and, consequently, the integrands of Eq. (7) must be analogous. This is easily seen in comparing the profiles of the difference between of the normal and tangential components of the pressure tensor in mixtures with different values of $\varepsilon_{22}/\varepsilon_{11}$. At the same thickness of the interface the maximums of the dependencies $P_N^*(z^*)$-$P_T^*(z^*)$, as their characteristic points, have similar values at equal concentrations c_l from the range from 0 to 0.02.

An analysis of the evolution of the profile of the difference between the normal and tangential components of the pressure tensor at $T^* = 0.9$ in a system with intensive adsorption ($\varepsilon_{22}/\varepsilon_{11} = 0.2$) shows that on the interval of concentrations from $c_l = 0$ to 0.212 the value of the maximum of the dependence $P_N^*(z^*)$-$P_T^*(z^*)$ decreases 30 times. At the same time, the interface expanded approximately 3.2 times (from $L_{10}^{*90} = 3$ to 9.5, Fig. 11). Owing to this, the surface tension, as the integral of $P_N^*(z^*)$-$P_T^*(z^*)$, decreased monotonically with the growth of c_l.

At $T^* = 0.9$ in a mixture with a larger asymmetry of interactions ($\varepsilon_{22}/\varepsilon_{11} = 0.1$) and weaker adsorption, in the range of existence of states of two-phase equilibrium from $c_l = 0$ to 0.057 the value of the maximum of the dependence $P_N^*(z^*)$-$P_T^*(z^*)$ decreased only 1.5 times. In this case the effective thickness of the interface increased approximately 1.6 times. At a concentration $c_l = 0.0375$ the area under the curve $P_N^*(z^*)$-$P_T^*(z^*)$ had the smallest value, and further began to increase.

The dependence $\gamma(p_s)$ at different temperatures has also been investigated in such systems as H_2O–CO_2 [36], H_2O–H_2S [37], and H_2O–CH_4, [38,39]. At temperatures lower than the critical temperature of the volatile component $T_{2,c}$ and those close to it the isotherms $\gamma(p_s)$ consist of two sections, which are approximated by linear functions with larger and smaller slopes. The rapid drop of surface tension with increasing pressure is terminated abruptly at a certain pressure, and further the surface tension decreases much more slowly. At every temperature below $T_{2,c}$ the pressure at which the slope of dependence $\gamma(p_s)$ changes abruptly corresponds to the

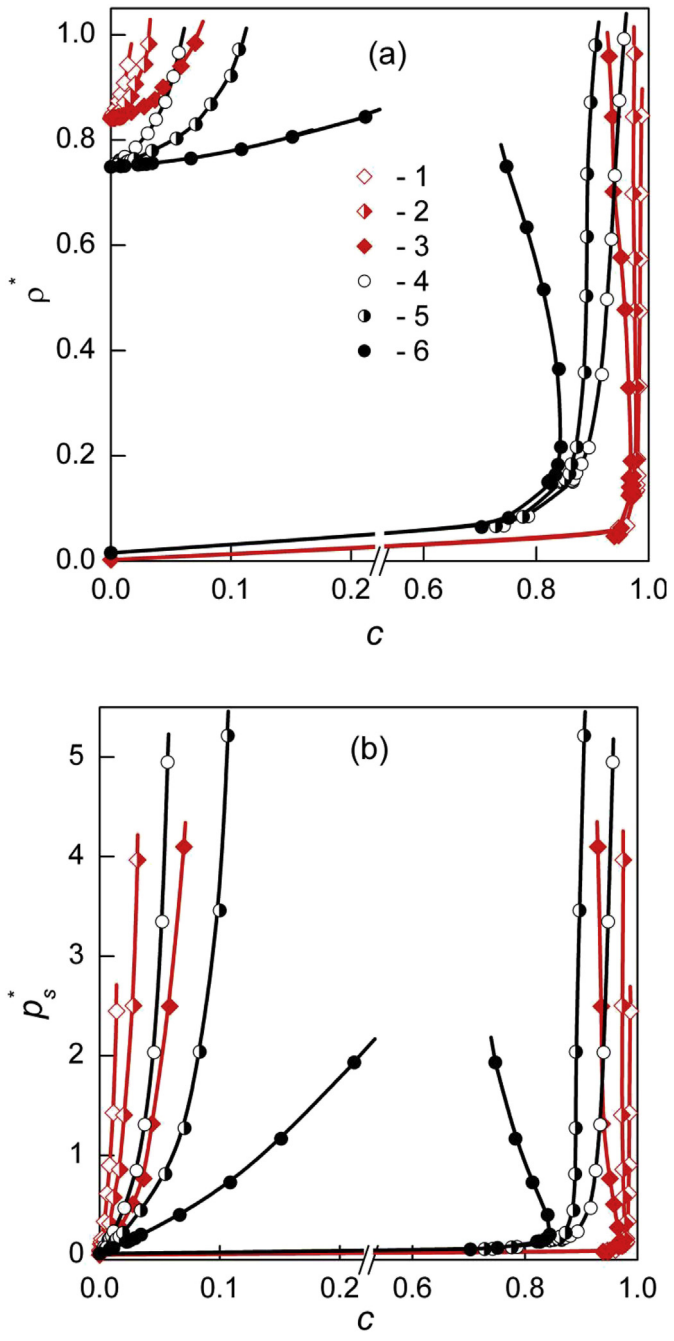

Fig. 8. Effect of the ratio $\varepsilon_{22}/\varepsilon_{11}$ on concentration dependences of orthobaric densities (a) and saturation pressure (b) at temperatures $T^* = 0.7$ (diamonds) and $T^* = 0.9$ (circles): (1, 4) $\varepsilon_{22}/\varepsilon_{11} = 1/10$; (2, 5) 1/7; (3, 6) 1/5.

pressure of a gas-liquid transition of the volatile component. Subcritical isotherms of $\gamma(p_s)$ with two sections reflect liquid-gas and liquid-liquid surface tension below and above this pressure.

At $T > T_{2,c}$ no phase transition is observed in a phase which is rich in the volatile component, and the isotherms $\gamma(p_s)$ in the supercritical region of existence of the second component exhibit a gradual reduction of the slope with increasing pressure.

In the H_2O–CH_4 mixture at saturation pressures up to 280 MPa and temperatures exceeding the critical temperature of methane more than twice on the $\gamma(p_s)$ isotherms there are minimums, after which the surface tension increases slightly with a further growth in p_s [39]. The nonmonotonic dependence $\gamma(p_s)$ in the H_2O–CH_4 mixture has been obtained by the DGT method [40]. A similar behavior is demonstrated by the dependences $\gamma(p_s)$ and $\gamma(c_l)$ obtained by us (see. Fig. 10b).

The increase of the surface tension in the H_2O–CH_4 system at high pressures and temperatures is explained in Ref. [40] on the basis of the results of MD simulations [41]. In Ref. [41] it is shown that at high temperatures hydrogen bonds weaken, which increases the mutual penetration of methane and water molecules and leads to a roughening of the interface. These two effects are enhanced at high pressures and ensure an increase in surface tension.

In the mixtures of one-atom LJ particles investigated by us one can also observe an intensification of the mutual penetration of particles of the volatile component and the solvent with increasing pressure. This is clearly demonstrated in Fig. 4 by the evolution of density profiles with an increase in the concentration of the volatile component (equilibrium pressure). In this case the narrowest interface takes place in the system with a ratio $\varepsilon_{22}/\varepsilon_{11} = 0.1$. It is for this mixture that the non-monotony of the dependences $\gamma(c_l)$ and $\gamma(p_s)$ is expressed most clearly (Fig. 10b).

4. Discussion

In diluted solutions the relation between the adsorption of the component 2 at the equimolecular dividing surface of the component 1 and the surface tension is established by the equation

$$\Gamma_{2(1)} = -\left(\frac{\partial\gamma}{\partial c_l}\right)\frac{c_l(1-c_l)}{k_BT}. \tag{11}$$

The results of calculation by Eq. (11) agree with data of MD simulation at small values of the concentration, where the isotherms of surface tension $\gamma(c_l)$ (Figs. 9 and 10) are close to straight lines. Thus, at a temperature $T^* = 0.9$ for systems with $\varepsilon_{22}/\varepsilon_{11} = 1/7$ and 1/5 the result of Eq. (11) within the error coincides with the data of Eq. (8) at $c_l < 0.02$ (Fig. 10b).

A qualitatively different behavior of concentration dependences of the relative adsorption of the volatile component has been obtained in Ref. [19]. At $0.4 \le \varepsilon_{22}/\varepsilon_{11} \le 0.7$ ($\sigma_{22} = \sigma_{11}$) in the range of c_l from 0 to 0.2 the relative adsorption $\Gamma_{2(1)}(c_l)$ on an isotherm increases almost linearly. On lines of constant concentration to smaller $\varepsilon_{22}/\varepsilon_{11}$ correspond larger values of relative adsorption. As $\varepsilon_{22}/\varepsilon_{11}$ decreases, one can observe the deviation of the curves $\Gamma_{2(1)}(c_l)$ from linearity, and at $\varepsilon_{22}/\varepsilon_{11} = 0.3$ the dependence $\Gamma_{2(1)}(c_l)$ exhibits a maximum [19]. In our calculations $\Gamma_{2(1)}(c_l)$ at a constant temperature decreases with decreasing $\varepsilon_{22}/\varepsilon_{11}$ and have the maximums when $\varepsilon_{22}/\varepsilon_{11} \le 0.2$.

Let us compare the results of our simulation with experimental data on Ar–Ne and Ar–He solutions, whose interatomic interactions are satisfactorily described by the Lennard-Jones potential. In the solutions mentioned neon and helium act as volatile components. For the Ar–Ne $\varepsilon_{22}/\varepsilon_{11} \approx 0.3$, for Ar–He ≈ 0.05. The ratio of the sizes of neon and helium atoms to that of argon atoms is not less than 0.75. Dissolution of 1% neon in argon at normal boiling temperature increases the saturation pressure by 1.1 Mpa, and dissolution of the same amount of helium, by 12 MPa [42]. A similar relative increase in the saturation pressure has been obtained in our model systems with $\varepsilon_{22}/\varepsilon_{11} = 0.2$ and 0.1 (see Fig. 8). At a constant temperature the surface tension of Ar–Ne solution decreases linearly with an increase in the neon concentration in the bulk liquid to $c_l = 0.06$ [42]. The isotherms $\gamma(c_l)$, obtained in MD simulation of mixtures with $\varepsilon_{22}/\varepsilon_{11} = 0.2$ and 0.1 contain sections close to linear ones when $c_l < 0.02$. At the same concentrations an increase in the relative adsorption is observed (Fig. 10). The isotherms $\Gamma_{2(1)}(c_l)$ calculated from experimental data on surface tension [42] in

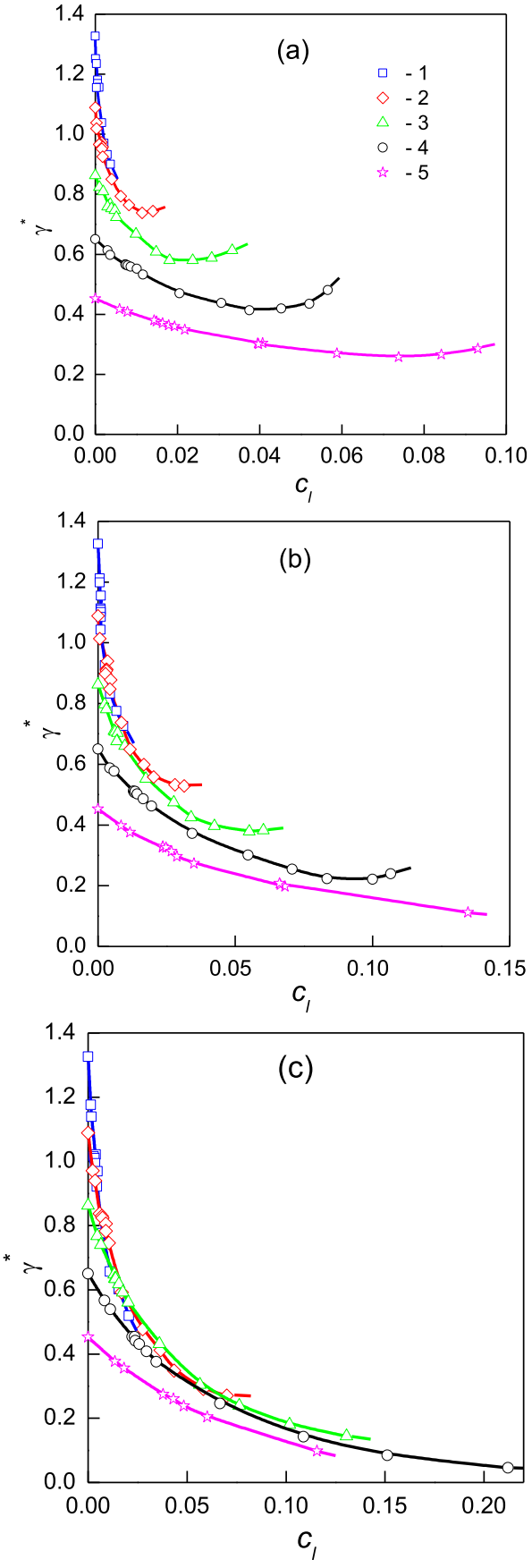

Fig. 9. Isotherms of surface tension versus the concentration of the second component in a bulk liquid. For symbols see Fig. 6.

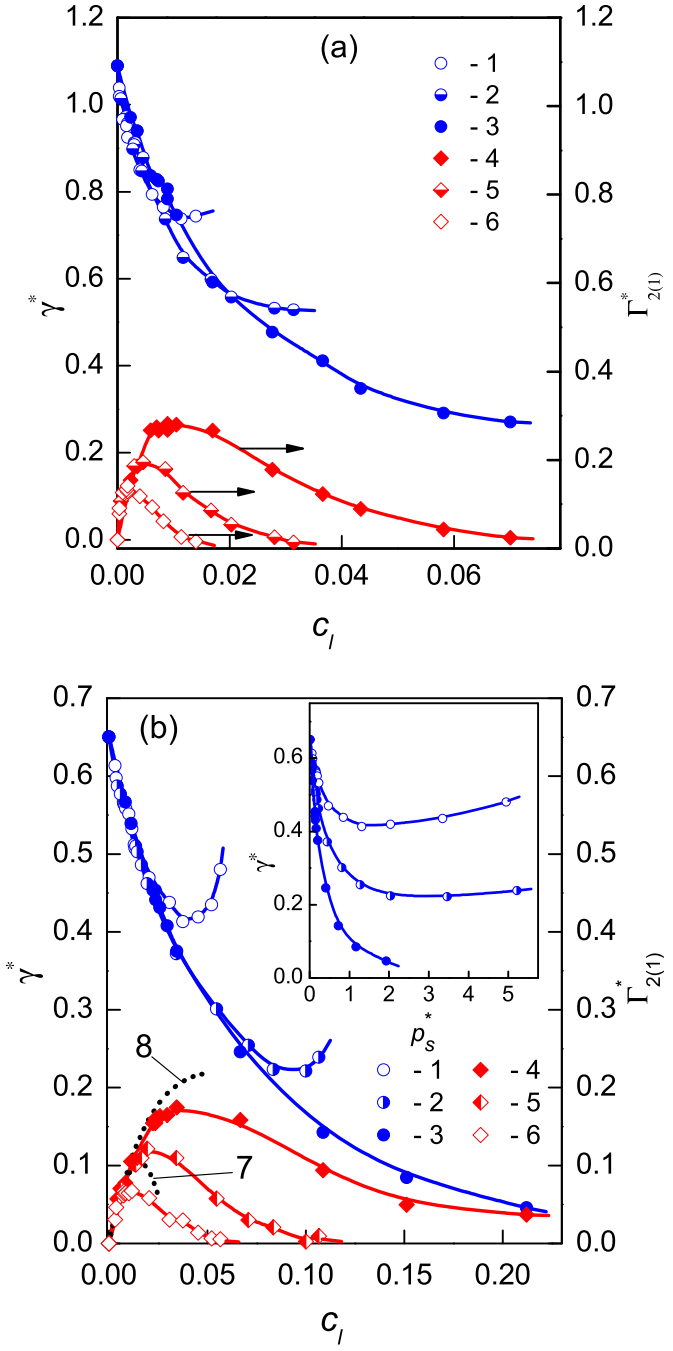

Fig. 10. Concentration dependences of surface tension (circles) and relative adsorption (diamonds) at $T^* = 0.7$ (a) and $T^* = 0.9$ (b) for the following ratios $\varepsilon_{22}/\varepsilon_{11}$: (1, 4) $\varepsilon_{22}/\varepsilon_{11} = 1/10$; (2, 5, 7) 1/7; (3, 6, 8) – 1/5. Dashed curves show calculation by Eq. (11). The inset shows dependences of surface tension on the saturation pressure.

accordance with Eq. (11) have only linear sections.

In experiments on diluted solutions Ar–H_2, Ar-D_2, Ar–Ne, Ar-He [42,43] it has been found that with increasing content of the low boiling component the value of the decrease in the surface tension is practically independent of the kind of the gas being dissolved. At low concentrations of the volatile component this is connected with the similarity of deviations from ideality of the solutions investigated. In the mixtures investigated by us the decrease of γ with the growth c_l is also independent of the value of $\varepsilon_{22}/\varepsilon_{11}$ at small values of c_l (Fig. 10).

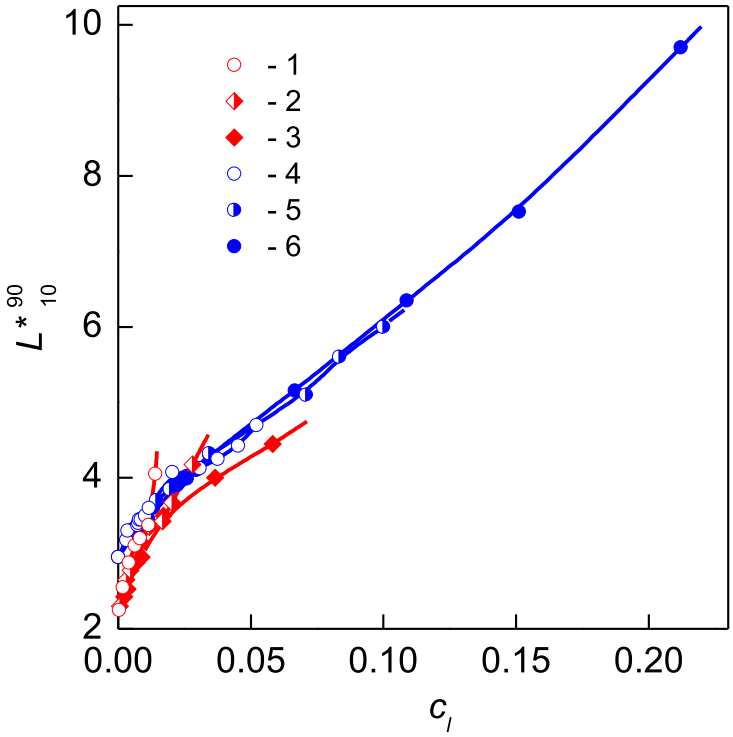

Fig. 11. Dependence of the effective thickness of the interface L^{*90}_{10} on the concentration of the second component in the bulk liquid at temperatures $T^* = 0.7$ (diamonds) and $T^* = 0.9$ (circles) for the following ratios $\varepsilon_{22}/\varepsilon_{11}$: (1, 4) $\varepsilon_{22}/\varepsilon_{11} = 1/10$; (2, 5) 1/7; (3, 6) – 1/5.

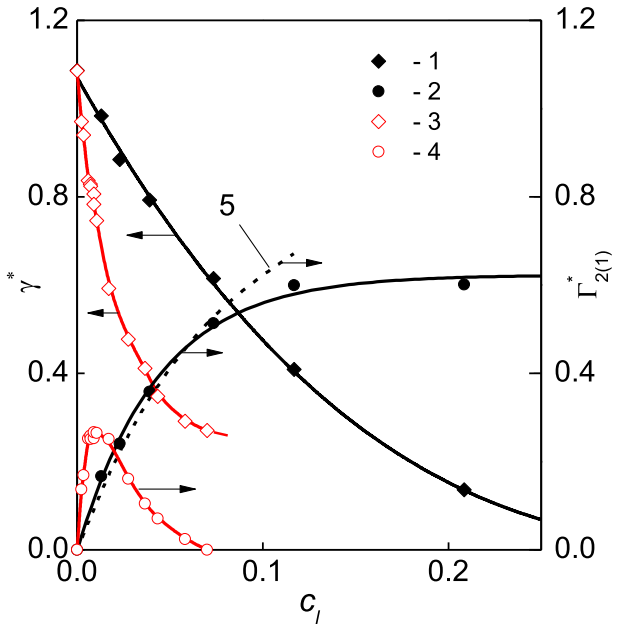

Fig. 12. Surface tension and relative adsorption of the volatile component at a temperature $T^* = 0.7$: (1, 2) Ar–Ne system [3], calculations γ^* by Eq. (7) and $\Gamma^*_{2(1)}$ by Eq. (8); (3, 4) mixture with $\varepsilon_{22}/\varepsilon_{11} = 0.2$, $\sigma_{22} = \sigma_{11}$, calculations by Eqs. (7) and (8); (5) calculation of $\Gamma^*_{2(1)}$ in an Ar–Ne system by Eq. (11).

Experimental data on the surface tension of Ar–Ne solution have been obtained with $c_l \leq 0.06$ [42,43]. MD simulation of a two-phase Ar–Ne mixture has been conducted in a wider range of concentrations of the volatile component ($c_l \leq 0.21$) [3]. Fig. 12 compares the dependences $\gamma^*(c_l)$ and $\Gamma^*_{2(1)}(c_l)$ at $T^* = 0.7$, obtained in Ref. [3], and in simulating a mixture with a ratio $\varepsilon_{22}/\varepsilon_{11} = 0.2$. In both systems, $\gamma^*(c_l)$ is a decreasing function, however in a mixture with $\varepsilon_{22}/\varepsilon_{11} = 0.2$ and equal-sized particles the decrease of $\gamma^*(c_l)$ proceeds about two times faster.

The dependencies $\Gamma^*_{2(1)}(c_l)$ in the Ar–Ne system and in the model with $\varepsilon_{22}/\varepsilon_{11} = 0.2$ are qualitatively different. An increase in the relative adsorption of the volatile component is observed in both solutions, however in the mixture with $\varepsilon_{22}/\varepsilon_{11} = 0.2$ this takes place in a range of concentrations c_l an order smaller than in the Ar–Ne system. An even more significant difference in the behavior of $\Gamma^*_{2(1)}(c_l)$ lies in the fact that in the Ar–Ne model the isotherm $\Gamma^*_{2(1)}(c_l)$ is a monotonic function, and in the case of mixtures with $\varepsilon_{22}/\varepsilon_{11} = 0.2$ and $\sigma_{22} = \sigma_{11}$ the increase of $\Gamma^*_{2(1)}(c_l)$ is limited by the maximum, after passing of which the relative adsorption drops to values close to zero.

5. Conclusion

Thus, the combination of highly asymmetric interparticle interactions of the components ($0.1 \leq \varepsilon_{22}/\varepsilon_{11} \leq 0.2$) and the equality of the particle sizes are responsible for the fact that the isotherms of relative adsorption in such mixtures depend nonmonotonically on the concentration of the volatile component in the liquid phase. Besides, in the interval of values of $\varepsilon_{22}/\varepsilon_{11}$ mentioned the relative adsorption at a fixed temperature decreases with decreasing $\varepsilon_{22}/\varepsilon_{11}$, as distinct from the inverse dependence of $\Gamma^*_{2(1)}$ on $\varepsilon_{22}/\varepsilon_{11}$ obtained in Ref. [19] at $0.4 \leq \varepsilon_{22}/\varepsilon_{11} \leq 0.7$.

Under changes of the composition of a binary mixture and redistribution of the components between the coexisting phases and the interface, one may observe cases where the dependence of the surface tension on the composition of one of the phases is of qualitatively different character for different intervals of the composition, and on the surface tension isotherm there is an extremum [44]. The isotherms $\gamma(c_l)$ obtained in experimental investigations of solutions with complete [45–47] and limited

[42,48,49] miscibility of the components, whose interactions may be satisfactorily described in the framework of the LJ model, have no extremums. Surface tension extremums were observed in systems with more complicated structures of the molecules of the components, for example, phenol-pyridine, phenol-methylamine [44], water-methane [39,40], and some others [50]. As a result of simulation, it has been established that in an LJ solution whose components differ only in the energy parameters of interaction more than 5 times, the concentration dependence of the surface tension may also have an extremum (minimum). As seen from a comparison of our results and those of experimental and theoretical investigations [30–40], the LJ model is rather universal. LJ model reproduces qualitatively and predicts the behavior of interfacial properties of H_2O–CO_2, H_2O–H_2S, H_2O–CH_4 mixtures at high pressures despite the fact that the interactions of atoms in such systems are described in a more complicated way.

Acknowledgements

The work has been performed with the financial support of the Program of Basic Research of the Ural Branch of the Russian Academy of Sciences, No. 7 (project 15-7-12-8) and the Russian Foundation for Basic Research (project 15-08-03399). The authors are grateful the Joint Supercomputer Center of RAS and the Supercomputing Center of the Institute of Mathematics and Mechanics of UB of RAS for kindly providing the computer facilities employed in performing this work.

References

[1] M. Mecke, J. Winkelmann, J. Fischer, Molecular dynamics simulation of the liquid–vapor interface: binary mixtures of Lennard-Jones fluids, J. Chem. Phys. 110 (1999) 1188–1192.
[2] E. Dıaz-Herrera, J. Alejandra, G. Ramırez-Santiago, F. Forstmann, Interfacial tension behavior of binary and ternary mixtures of partially miscible Lennard-Jones fluids: a molecular dynamics simulation, J. Chem. Phys. 110 (1999) 8084–8089.
[3] V.G. Baidakov, S.P. Protsenko, Molecular-dynamics investigation of phase equilibrium and surface tension in argon-neon system, J. Phys. Chem. C 112 (2008) 17231–17234.
[4] E. Diaz-Herrera, G. Ramirez-Santiago, J.A. Moreno-Razo, Phase and interfacial behavior of partially miscible symmetric Lennard-Jones binary mixtures, J. Chem. Phys. 123 (2005), 184507(9).
[5] V.I. Harismiadis, N.K. Koutras, D.P. Tassios, A.Z. Panagiotopoulos, How good is conformal solution theory for phase equilibrium predictions? Gibbs ensemble simulations of binary Lennard-Jones mixtures, Fluid Phase Equilib. 65 (1991) 1–18.
[6] V.I. Harismiadis, A.Z. Panagiotopoulos, D.P. Tassios, Phase equilibria of binary Lennard-Jones mixtures with cubic equation of state, Fluid Phase Equilib. 94 (1994) 1–18.
[7] A.M. Georgoulaki, I.V. Ntouros, D.P. Tassios, A.Z. Panagiotopoulos, Phase equilibria of binary Lennard-Jones mixtures: simulation and van der Waals l-fluid theory, Fluid Phase Equilib. 100 (1994) 153–170.
[8] J.N. Canongia Lopes, Phase equilibria in binary Lennard-Jones mixtures: phase diagram simulation, Mol. Phys. 96 (1999) 1649–1658.
[9] V.F. Cabral, R.R.C. Pinto, F.W. Tavares, M. Castier, Phase equilibria of binary mixtures by molecular simulation and cubic equations of state, Braz. J. Chem. Eng. 18 (2001) 149–161.
[10] J.J. Potoff, A.Z. Panagiotopoulos, Critical point and phase behavior of the pure fluid and a Lennard-Jones mixture, J. Chem. Phys. 109 (1998) 10914–10920.
[11] J.D. van der Waals, Ph Kohnstamm, Lehrbuch der Thermodynamik, first ed., Maasand van Suchtelen, Amsterdam, 1908.
[12] J.W. Cahn, J.E. Hilliard, Free energy of a nonuniform system. I. Interfacial free energy, J. Chem. Phys. 28 (1958) 258–267.
[13] H.T. Davis, L.E. Scriven, Stress and structure in fluid interfaces, Adv. Chem. Phys. 49 (1982) 357–454.
[14] V.G. Baidakov, M.N. Khotienkova, Surface tension of methane-nitrogen solutions: 2. Description in the framework of the van der Waals gradient theory, Fluid Phase Equilib. 425 (2016) 402–410.
[15] V. Bonjiorno, H.T. Davis, Modified Van der Waals theory of fluid interfaces, Phys. Rev. A 12 (1975) 2213–2224.
[16] R. Evans, The nature of the liquid-vapor interface and other topics in the statistical mechanics of non-uniform, classical fluids, Adv. Phys. 28 (1979) 143–200.
[17] I.W. Plesner, O. Platz, S.E. Christiansen, Statistical mechanical calculation of surface properties of simple liquids and liquid mixtures. II. Mixtures, J. Chem. Phys. 48 (1968) 5364–5370.
[18] D.J. Lee, M.M. Telo da Gama, K.E. Gubbins, The vapour-liquid interface for a Lennard-Jones model of argon-krypton mixtures, Mol. Phys. 53 (1984) 1113–1130.
[19] D.J. Lee, M.M. Telo da Gama, K.E. Gubbins, Adsorption and surface tension reduction at the vapor-liquid interface, J. Phys. Chem. 89 (1985) 1514–1519.
[20] A.Z. Panagiotopoulos, Direct determination of phase coexistence properties of fluids by Monte Carlo simulation in a new ensemble, Mol. Phys. 61 (1987) 813–826.
[21] A.Z. Panagiotopoulos, N. Quirke, M. Stapletion, D.J. Tildesley, Phase equilibria by simulation in the Gibbs ensemble: alternative derivation, generalization and application to mixture and membrane equilibria, Mol. Phys. 63 (1988) 527–545.
[22] B. Smit, Ph de Smedt, D. Frenkel, Computer simulation in the Gibbs ensemble, Mol. Phys. 68 (1989) 93l–950.
[23] J.O. Hirschfelder, C.F. Curtiss, R.B. Bird, Molecular Theory of Gases and Liquids, Wiley, New York, 1954.
[24] V.G. Baidakov, G.G. Chernykh, S.P. Protsenko, Effect of the cut-off radius of the intermolecular potential on phase equilibrium and surface tension in Lennard-Jones systems, Chem. Phys. Lett. 321 (2000) 315–320.
[25] S. Nose, M.L. Klein, Constant pressure molecular dynamics for molecular systems, Mol. Phys. 50 (1983) 1055–1076.
[26] S. Nose, A molecular dynamics method for simulations in the canonical ensemble, Mol. Phys. 52 (1984) 255–268.
[27] W.G. Hoover, Canonical dynamics: equilibrium phase-space distributions, Phys. Rev. A 31 (1985) 1695–1697.
[28] J.P.R.B. Walton, D.J. Tildesley, J.S. Rowlinson, J.R. Henderson, The pressure tensor at the planar surface of a liquid, Mol. Phys. 48 (1983) 1357–1368.
[29] J. Lekner, J.R. Henderson, Theoretical determination of the thickness of a liquid-vapor interface, Physica 94A (1978) 545–558.
[30] Xia-osen Li, Jian-min Liu, Dong Fu, Investigation of interfacial tensions for carbon dioxide aqueous solutions by perturbed chain statistical associating fluid theory combined with density-gradient theory, J. Ind. Eng. Chem. Res. 47 (2008) 8911–8917.
[31] T. Lafitte, B. Mendiboure, M.M. Piñeiro, D. Bessieres, C. Miqueu, Interfacial properties of water/CO2: a comprehensive description through a gradient theory - SAFT-VR Mie approach, J. Phys. Chem. B 114 (2010) 11110–11116.
[32] O.G. Nino-Amezquita, Interfacial Properties and Phase Equilibria for Mixtures Relevant in the Oil and Gas Industry, 2014. Thesis Dr.-Ing., Berlin.
[33] S. Khosharay, F. Varaminian, Experimental and modeling investigation on surface tension and surface properties of (CH4 + H2O), (C2H6 + H2O), (CO2 + H2O) and (C3H8 + H2O) from 284.15 K to 312.15 K and pressures up to 60 bar, Int. J. Refrig. 47 (2014) 26–35.
[34] S. Khosharay, M. Abolala, F. Varaminian, Modeling the surface tension and surface properties of (CO2+H2O) and (H2S + H2O) with gradient theory in combination with sPC–SAFT EOS and a new proposed influence parameter, J. Mol. Liq. 198 (2014) 292–298.
[35] Y.T.F. Chow, D.K. Eriksen, A. Galindo, A.J. Haslam, G. Jackson, G.C. Maitland, J.P.M. Trusler, Interfacial tensions of systems comprising water, carbon dioxide and diluent gases at high pressures: experimental measurements and modelling with SAFT-VR Mie and square-gradient theory, Fluid Phase Equilib. 407 (2016) 159–176.
[36] A. Georgiadis, G. Maitland, J.P.M. Trusler, A. Bismarck, Interfacial tension measurements of the (H_2O + CO_2) system at elevated pressures and temperatures, J. Chem. Eng. Data 55 (2010) 4168–4175.
[37] V. Shah, D. Broseta, G. Mouronval, F. Montel, Water/acid gas interfacial tensions and their impact on acid gas geological storage, Int. J. Greenh. Gas Control 2 (2008) 594–604.
[38] H.Y. Jennings Jr., G.H. Newman, The effect of temperature and pressure on the interfacial tension of water against methane-normal decane mixtures, Soc. Petrol. Eng. J. 11 (1971) 171–175.
[39] G. Wiegand, E.U. Franck, Interfacial tension between water and non-polar fluids up to 473 K and 2800 bar, Bunsen Phys. Chem. 98 (1994) 809–817.
[40] K.A.G. Schmidt, G.K. Folas, B. Kvamme, Calculation of the interfacial tension of the methane–water system with the linear gradient theory, Fluid Phase Equilib. 261 (2007) 230–237.
[41] B. Kvamme, T. Kuznetsova, K.A.G. Schmidt, Experimental measurements and numerica l modelling of in terfacial tension in water-methane systems, in: Proceedings of the 4th WSEAS International Conference on Heat and Mass Transfer, Gold Coast, Queensland, Australia, January 17-19, 2007, pp. 20–26.
[42] A.M. Kaverin, V.N. Andbaeva, V.G. Baidakov, Surface tension at the boundaries of helium-argon and neon-argon solutions at 108-140 K, Rus. J. Phys. Chem. 80 (2006) 413–417.
[43] YuP. Blagoy, Investigations of Thermodynamic Properties of Liquefied Gases and Their Solutions, 1970. Thesis … Doctor of Physics and Mathematics, Kharkov.
[44] A.I. Rusanov, Phasengleichgewichte und grenzflachenerscheinungen, Akademie-Verlag, Berlin, 1978.
[45] V.G. Baidakov, A.M. Kaverin, V.N. Andbaeva, The liquid-gas interface of oxygen-nitrogen solutions 1. Surface tension, Fluid Phase Equilib. 270 (2008) 116–120.
[46] V.G. Baidakov, M.N. Khotienkova, V.N. Andbaeva, A.M. Kaverin, Capillary constant and surface tension of methane-nitrogen solutions: 1. Experiment, Fluid Phase Equilib. 301 (2011) 67–72.

[47] V.G. Baidakov, A.M. Kaverin, M.N. Khotienkova, V.N. Andbaeva, Surface tension of an ethane-nitrogen solution: 1. Experiment and thermodynamic analysis of the results, Fluid Phase Equilib. 328 (2012) 13–20.
[48] V.G. Baidakov, I.I. Sulla, Surface tension of helium- oxygen and helium-ethane solutions, Int. J. Thermophys 16 (1985) 909–926.
[49] V.G. Baidakov, K.A. Grishina, Capillary constant and surface tension of methane-helium solution, Fluid Phase Equilib. 354 (2013) 245–249.
[50] R. Defay, I. Prigogine, Surface Tension and Adsorption, Wiley, New York, 1966.

Nomenclature

A: surface area of one interface
$\langle c \rangle$: average concentration (molar fraction) of the second component in the mixture
c_l: concentration of the second component in the bulk liquid
c_g: concentration of the second component in the gas
k_B: Boltzmann constant
L_x, L_y, L_z: length of cell along x, y, and z axis, respectively
L_{10}^{90}: thickness of the interface
m: mass of particle
N: number of particles
p_s: saturation pressure
P_N: normal component of the pressure tensor
P_T: tangential component of the pressure tensor
r: distance between the two particles
r_c: cutoff radius of interaction
t: time
Δt: integration timestep of the equations of motion
T: temperature
T_c: critical temperature
u: density of potential energy
V: cell volume
x_{ij}, y_{ij}, *and* z_{ij}: the separations of particles i and j along x, y, and z axis
v: velocity of particle $z_{1,e}$ position of the equimolecular dividing surface of the first component
Δz: thickness of layer in calculation of profiles

Greek letters

ε: energy parameter of LJ potential
ϕ: interaction energy
$\Gamma_{2(1)}$: relative adsorption of the second component
γ: surface tension
ρ: number density
$\Delta\rho$: difference between orthobaric densities of liquid and gas
σ: size parameter of LJ potential

Subscripts

1: first component of mixture
2: second component
α: number of component of mixture
β: number of component of mixture
g: gas
l: liquid
n: number of layer along x axis

Superscripts

*: reduced values